JOURNAL OF VIROLOGY, Mar. 2008, p. 2989–2999 Vol. 82, No. 6
0022-538X/08/$08.00+0 doi:10.1128/JVI.01906-07

Envelope Protein Palmitoylations Are Crucial for Murine Coronavirus Assembly[▽]

Joseph A. Boscarino, Hillary L. Logan, Jason J. Lacny, and Thomas M. Gallagher*

Department of Microbiology and Immunology, Loyola University Medical Center, Maywood, Illinois

Received 31 August 2007/Accepted 28 December 2007

The coronavirus assembly process encloses a ribonucleoprotein genome into vesicles containing the lipid-embedded proteins S (spike), E (envelope), and M (membrane). This process depends on interactions with membranes that may involve palmitoylation, a common posttranslational lipidation of cysteine residues. To determine whether specific palmitoylations influence coronavirus assembly, we introduced plasmid DNAs encoding mouse hepatitis coronavirus (MHV) S, E, M, and N (nucleocapsid) into 293T cells and found that virus-like particles (VLPs) were robustly assembled and secreted into culture medium. Palmitate adducts predicted on cysteines 40, 44, and 47 of the 83-residue E protein were then evaluated by constructing mutant cDNAs with alanine or glycine codon substitutions at one or more of these positions. Triple-substituted proteins (E.Ts) lacked palmitate adducts. Both native E and E.T proteins localized at identical perinuclear locations, and both copurified with M proteins, but E.T was entirely incompetent for VLP production. In the presence of the E.T proteins, the M protein subunits accumulated into detergent-insoluble complexes that failed to secrete from cells, while native E proteins mobilized M into detergent-soluble secreted forms. Many of these observations were corroborated in the context of natural MHV infections, with native E, but not E.T, complementing debilitated recombinant MHVs lacking E. Our findings suggest that palmitoylations are essential for E to act as a vesicle morphogenetic protein and further argue that palmitoylated E proteins operate by allowing the primary coronavirus assembly subunits to assume configurations that can mobilize into secreted lipid vesicles and virions.

Coronavirus-infected cells provide models to investigate protein targeting, subcellular protein transport, protein-lipid and protein-protein interactions, and of multiprotein complex assembly. This is because all of these events take place efficiently and in organized temporal fashion within cells to create infectious, lipid-enveloped virus particles. The essential components of infectious coronavirions include three membrane proteins, S (spike), E (envelope), and M (membrane), along with cytoplasmic N (nucleocapsid). These four proteins, along with newly synthesized monopartite plus-strand RNA virus genomes, congregate at endoplasmic reticulum and Golgi membranes, ultimately remodeling the membranes such that they intrude inward toward organelle lumen and then undergo membrane fission to create enveloped virus vesicles. Accomplishing these morphological changes involves several well-known interactions. N proteins bind viral RNAs to generate helical ribonucleoprotein (RNP) complexes (27), RNPs in turn bind to the cytoplasmic carboxyl-terminal extensions of M proteins (25, 45), M proteins bind to each other (9), and M and S proteins interact at or near their transmembrane-spanning regions (10, 16, 57). Subcellular targeting signals in the S, E, and M proteins interacting with presumed cellular factors restrict associations to intracellular membrane environments (3, 30, 49).

One of the more enigmatic associations in this assembly process involves the E proteins. Despite the fact that E proteins are in virions (58) and that physical interactions between E and M have been documented previously (4, 28), it appears increasingly likely that E proteins are not classical essential virion assembly subunits. Indeed, E proteins foster coronavirus assembly but are not absolutely required; recombinant murine hepatitis coronaviruses (rMHVs) and recombinant severe acute respiratory syndrome (SARS) viruses lacking functional E genes are significantly attenuated but are nonetheless viable (6, 26). Additionally, E proteins of several different coronaviruses, despite having amino acid identities of only about 20%, will substitute for MHV E and provide robust growth to rMHV lacking E (24). Therefore, E proteins cannot be obligate virion assembly subunits with type-specific interacting assembly partners.

These results suggest that a greater understanding of the E proteins may come from studying E interactions with the membranes that are common to all the assembly processes, inasmuch as studying type-specific protein-protein interactions may be less relevant. E proteins are indeed membrane morphogens. When synthesized alone, E proteins reconfigure intracellular membranous organelles into elongated swirls (44) and will even induce the secretion of exosomal vesicles if overexpressed (33). In coexpression with M proteins, E and M form extracellular vesicles in which both proteins reside (51).

These membrane morphogenetic capabilities are achieved by very small proteins; the coronavirus E proteins range from 76 to 109 amino acids (Fig. 1). All E proteins evaluated to date have an uncleaved, N-terminal, ~30-residue hydrophobic region that confers membrane association (44) and a C-terminal hydrophilic region that resides cytoplasmically, i.e., within virion interiors in so-called "C-endo" orientation (34). It is not clear whether the N-terminal region acts as a "type III" signal/

* Corresponding author. Mailing address: Department of Microbiology and Immunology, Loyola University Medical Center, 2160 South First Avenue, Maywood, IL 60153. Phone: (708) 216-4850. Fax: (708) 216-9574. E-mail: tgallag@lumc.edu.

▽ Published ahead of print on 9 January 2008.

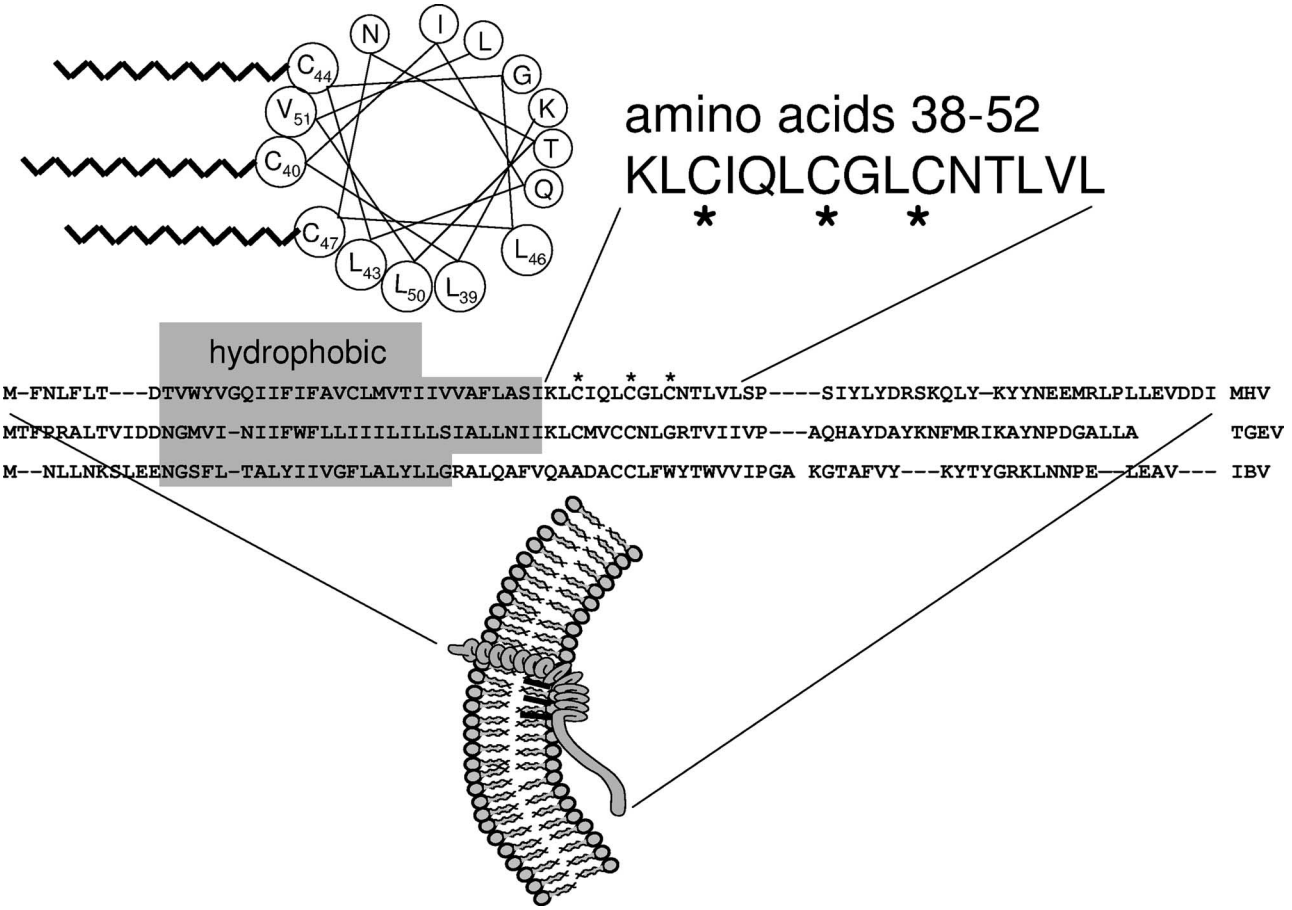

FIG. 1. Features of coronavirus E proteins. The cysteine-rich region of the MHV E protein (residues 38 to 52) is depicted in a helical wheel format. Hydrophobic residues of the helical wheel are identified with large encircled shading, and palmitates extending from cysteines 40, 44, and 47 are depicted with corrugated lines. Cysteines 40, 44, and 47 are denoted with asterisks in the primary sequence. Residues 38 to 52 are delineated in the context of the entire E amino acid sequence and compared with E sequences for groups 1 (TGEV) and 3 (IBV). The membrane-intercalating portions of each E protein are highlighted. A predicted membrane organization for the MHV E protein is illustrated at the bottom, in the context of a budding virion, with the outside of the virion at left and the inside at right. See the text for additional details.

anchor motif and thus promotes the translocation of the entire N terminus (i.e., to "N-exo" orientation) or whether this long N region inserts polytopically in a hairpin-type configuration in the bilayer, leaving N-endo termini. However, the N-exo orientation might be considered more likely, as the unusually long hydrophobic stretch is a feature favoring membrane translocation of N termini (52), as are the positive charges following this hydrophobic span (22). In addition to these positively charged amino acids, the C-terminal endoplasmic regions exhibit distinctive features, notably a conserved proline that is 16 to 20 residues from the end of the hydrophobic region. This 16- to 20-residue region between the hydrophobic span and the proline is termed a "cysteine-rich region" (47), as most of the E proteins contain a CxxxCxxC or CxxCxxxC motif near their centers. In this motif, shown in Fig. 1, the central cysteine residue is always conserved and is sometimes a dicysteine. Infectious bronchitis coronavirus (IBV) E proteins contain only this minimal CC, and one or both of these cysteines are posttranslationally modified with the 16-carbon aliphatic hydrocarbon palmitic acid, as evidenced by incorporation of radiolabeled palmitates during infection (3). Similar palmitoylated cysteines are likely present on MHV E proteins as well (58). Notably, bioinformatic predictions (www.bioinfo.tsinghua.edu.cn/NBA-Palm) suggest that all the cysteines residing within the E protein cysteine-rich regions of transmissible gastroenteritis coronavirus (TGEV) (a group 1 coronavirus), MHV and SARS virus (group 2), and IBV (group 3) are strong candidates for posttranslational palmitoylation.

The predicted propensity for the cysteine-rich region to adopt an alpha-helical secondary structure, the conserved 3- to 4-residue spacing of the cysteines, and the likelihood that these cysteines are modified by hydrophobic palmitate extensions immediately suggest a model in which the lipid adducts extend into cytoplasmic membrane leaflets from one face of an E protein helix (Fig. 1). In this model, the cysteine-rich region of E is held against the cytoplasmic side of the membrane bilayer, perhaps with its putative helical register fixed into position relative to the membrane by the covalently linked lipids. We hypothesized that this putative palmitoylation-dependent E configuration on membranes would be necessary for E function during coronavirus assembly. This hypothesis was an extension from our earlier studies in which we discovered palmi-

toylation-dependent assembly of S proteins into coronavirus particles (50). We set out to test these ideas by developing model systems to dissect coronavirus assembly and by subsequently evaluating mutant E proteins with various cysteine substitutions for their virus particle morphogenetic capabilities.

MATERIALS AND METHODS

Cells. 17Cl1 fibroblasts were grown in Dulbecco's modified Eagle medium (DMEM) containing 5% tryptose phosphate broth (Difco Laboratories) and 5% heat-inactivated fetal bovine serum (FBS). Human epithelial kidney cells (293T) and *Felis catus* whole fetus (FCWF) cells were grown in DMEM supplemented with 10% FBS. All growth media included 0.01 M sodium HEPES (pH 7.4). Cell lines were propagated as adherent monolayer cultures.

Plasmid constructions and transfections. MHV genes encoding S, E, M, and N were PCR amplified using template pMH54-A59 (36). Forward and reverse primers included SacI and XmaI restriction sites, respectively. After SacI-XmaI digestion, restriction fragments were cloned into pCAGGS.MCS (38). Mutations in the pCAGGS-E constructs were created using mutagenic primers and a site-directed mutagenesis kit (QuikChange; catalog no. 200519-5; Stratagene). E mutations were designated as single (E.S) C40A, C44A, and C47A substitutions. Double (E.D) mutations were C40A/C44G. The triple (E.T) mutant used in this report was C40A/C44G/C47G. Codons for influenza virus hemagglutinin (HA) epitope were appended immediately following the final 3′ E sense codon using a reverse primer that included E sequences, the nine HA codons, and the XmaI restriction site, to encode the sequence **VDDI**YPYDVPDYA (E residues are bold). Following PCR amplification and SacI-XmaI digestion, PCR products were cloned into pCAGGS.MCS to create the pCAGGS-HA-tagged E (E_{HA}) constructs. All plasmid constructs were sequenced to confirm the presence of desired mutations.

Plasmid DNAs encoding the indicated virion proteins were mixed in equimolar ratios and brought to identical total DNA concentrations by adding empty plasmid vector DNA (designated as "V" in figures) and then precipitated using calcium phosphate and incubated with 293T cells (typically 4 μg of plasmid DNA applied to 10^6 cells in a 10-cm^2 dish) for 18 h. Transfection medium was then removed and replaced with complete DMEM-10% FBS. For transfection of 17Cl1 cells, 4 μg plasmid DNAs were mixed with 10 μg Lipofectamine 2000 (Invitrogen) in 1 ml Opti-MEM (catalog no. 11058; Gibco) and applied to 10^6 cells for 3 h and then removed and replaced with complete media.

Preparation of cell lysates. At 2 days posttransfection, medium (1 ml per 10-cm^2 dish) was removed from each culture and adherent cells were dissolved in 0.1 ml of lysis buffer (25 mM sodium HEPES [pH 7.4], 100 mM NaCl, 0.5% NP-40, 0.5% sodium deoxycholate, and 0.1% protease inhibitor cocktail [Sigma P2714]). Cell lysates were then clarified by centrifugation at 500 × *g* for 15 min. In some experiments, the lysates were further clarified by centrifugation at 20,000 × *g* for 15 min at 4°C. Supernatant fluids and pellets, designated as soluble and insoluble fractions, were further clarified by two additional centrifugation cycles involving the resuspension of insoluble material in the same volumes of lysis buffer and repelleting. Sodium dodecyl sulfate (SDS) was added to the final soluble and insoluble fractions to 0.1% concentration, vortexed vigorously to dissolve all proteins, and stored at −20°C. For electrophoretic analysis, samples were mixed with 1/6 volumes of 6× SDS sample solubilizer (1× SDS sample solubilizer is 50 mM Tris-HCl [pH 6.8], 100 mM dithiothreitol, 2% SDS, 10% glycerol, 0.01% bromophenol blue) and heated at 95°C for 5 min. Final samples typically contained 10^7 cell equivalents per milliliter.

Preparation of VLPs. Media were clarified by sequential 20-min centrifugations at 500 × *g* and 20,000 × *g*. One-milliliter volumes of clarified media were then overlaid onto 0.5-ml cushions of 30% (wt/wt) sucrose in HNB (25 mM Na-HEPES [pH 7.4], 100 mM NaCl, 0.01% bovine serum albumin [BSA]). Virus-like particles (VLPs) were pelleted through sucrose in the Beckman TLA-100.3 rotor at 200,000 × *g* for 15 min. Supernatants were decanted and discarded, and clean dry pellets resuspended in 0.1-ml volumes of either HNB or SDS sample solubilizer and stored at −20°C.

Immunoprecipitations. Clarified lysates (0.5 ml containing 5×10^5 cell equivalents) were mixed by inversion overnight at 4°C with 0.8 μg 12CA5 anti-HA antibody (Roche, Inc.) and then with 0.01-ml paramagnetic protein A beads (New England Biolabs) for an additional 2 h at 4°C. Beads were collected using a magnetic rack, supernatant fluids were aspirated and discarded, and beads were then rinsed by three successive cycles of resuspension and recollection with 1-ml volumes of lysis buffer. The final rinsed bead pellets were suspended in 0.06 ml of SDS sample solubilizer and heated at 95°C for 5 min. These final samples contained immunoprecipitated proteins at a concentration corresponding to 10^7 cell equivalents per milliliter.

Hydroxylamine treatments. Immunoprecipitated proteins in SDS sample solubilizer were divided into aliquots and mixed with equal volumes of either water or 1 M hydroxylamine (catalog no. 379921; Sigma) in water. Hydroxylamine stock was adjusted to pH 7.4. After 15 min at room temperature, samples were subjected to SDS-polyacrylamide gel electrophoresis (PAGE).

Electrophoresis and immunoblotting. Proteins associated with cell lysates, VLPs, and immunoprecipitated material were all subjected to SDS-PAGE and transferred to polyvinylidene difluoride membranes. In most experiments, electrophoresis conditions were such that the amounts of cell lysates and VLPs loaded per lane corresponded to equivalent proportions of each cell culture. Polyvinylidene difluoride membranes were blocked for 1 h with 5% nonfat milk powder in TBST (25 mM Tris-HCl [pH 7.5], 140 mM NaCl, 2.7 mM KCl, 0.05% Tween 20) and then incubated overnight in TBST-1% milk containing antibodies specific for S (monoclonal antibody [MAb] 10G [19]), N (MAb J.3.1 [15]), M (MAb J.1.3 [15]), and E (antiserum E-C [34]). In experiments involving E_{HA} forms, MAb HA.11 (Covance) was used. Bound antibodies were detected using secondary antibody-horseradish peroxidase conjugates and enhanced chemiluminescence reagents (Perkin-Elmer Co.).

Immunofluorescence and confocal microscopy. 17Cl1 cells were grown on glass coverslips to approximately 40% confluence, then transfected with empty pCAGGS, pCAGGS-E_{HA}, and pCAGGS-E.T_{HA}. Two hours later, cells were infected with MHV-A59 at 0.1 PFU per cell. At 8 h postinfection (hpi), cells were fixed in phosphate-buffered saline (PBS)-4% paraformaldehyde for 10 min and permeabilized in digitonin buffer (5 μg/ml digitonin in 300 mM sucrose, 100 mM KCl, 2.5 mM $MgCl_2$, 1 mM EDTA, 10 mM HEPES [pH 6.9]) for 15 min at room temperature. Fixed cells on coverslips were blocked with PBS-2% BSA and probed in PBS-2% BSA with a fluorescein isothiocyanate-conjugated antibody directed against the HA tag (HA-FITC; Immunology Consultants Laboratory) and mouse anti-N J.3.1. In a separate assay, E-transfected cells were left uninfected and processed as above at 24 h posttransfection by probing with anti-HA and anti-Golgin-97 (catalog no. A21270; Molecular Probes, Inc.). The coverslips were washed three times in ice-cold PBS at room temperature and incubated with a red fluorochrome-conjugated secondary antibody (Mouse-658; Molecular Probes) for 1 h at room temperature. The coverslips were again washed three times in PBS, stained with Hoechst 33258, and mounted with ProLong Gold antifade reagent (Invitrogen). Confocal images were captured using a Carl Zeiss model 510 laser-scanning confocal microscope. Digitized images were processed with Image J (National Institutes of Health), assembled, and labeled in Microsoft PowerPoint.

Recombinant virus production. rMHVs were created via targeted RNA recombination according to the methods developed by Kuo et al. (23) and Masters and Rottier (36). To begin, in vitro RNA transcription template pMH54 was modified at two sites. First, the gene for firefly luciferase (FL) was amplified from plasmid pGL3 (Promega, Inc.) using forward and reverse primers containing distal EcoRV restriction sites. Following EcoRV digestion, FL amplicons were cloned into pMH54 at its unique EcoRV site between E and M open reading frames. This approach to introduce the FL reporter gene was developed by de Haan et al. (8). Second, using mutagenic primers and overlap-extension PCR, the E ATG initiation codon was converted to TAG. Third, the E gene in pMH54 was replaced with E.T by using restriction fragment exchange. Following the nomenclature of de Haan et al. (8), the final constructs were designated pMH54-E-FL-M (FL between E and M genes), pMH54-Eko-FL-M (E with ATG-to-TAG substitutions), and pMH54-E.T-FL-M (E with C40A/C44G/C47G changes).

PacI-linearized pMH54-based template DNAs (2 μg) were in vitro transcribed using reagents and protocols from Ambion, Inc. (mMessage mMachine, catalog no. 1344; Ambion). RNAs (~10 μg) were then added to 0.8 ml of PBS containing ~2×10^7 feline MHV-infected FCWF cells and immediately electroporated using a Bio-Rad Gene Pulser II (two high-capacitance pulses at 950 μF/0.3 kV). Cells were then added to approximately 30% confluent 17Cl1 monolayers (25 cm^2) and incubated for 2 days. Media were collected, and amplified recombinant MHV strain A59 (rA59) viruses were isolated by two rounds of sequential plaque purification on 17Cl1 cells. Recombinant virus stocks were then grown on 17Cl1 cells, infectivities were determined by plaque assay, and mutations were confirmed by reverse transcription-PCR and sequencing.

Complementation and augmentation assays. 17Cl1 cells were lipofected with indicated pCAGGS-E plasmids, and 18 h later, cells were infected at ~0.004 PFU per cell with rA59-Eko-FL-M (for complementation) or rA59-E-FL-M (for augmentation). At 18 hpi, media were collected and the virus producer cells were dissolved in reporter lysis buffer (luciferase assay system, catalog no. E1501; Promega). Collected media were clarified by centrifugation at 500 × *g* for 10 min

and used to infect 17Cl1 target cells in 96-well plates. At 6 hpi, target cells were rinsed with saline and dissolved in reporter lysis buffer. Luminescence potentials were recorded after the injection of luciferase assay substrate into cell lysates and measurement of light emissions by using a Veritas microplate luminometer (Turner BioSystems). All transfections were performed in triplicate, and medium from each transfection was inoculated in quadruplicate onto target cells.

RESULTS

A robust system for evaluating MHV assembly. Several recent reports have revealed that pCAGGS (38) is a suitable plasmid DNA vector for expressing cDNAs encoding coronavirion-associated proteins (20). These reports prompted us to create four pCAGGS vectors encoding MHV (strain A59) S, E, M, and N, as this plasmid collection could potentially provide for VLP formation. Once the plasmid DNAs were generated, our plans were to use easily transfected cell lines such as human kidney 293T so that all four plasmids might be introduced simultaneously into cells at high efficiencies. We executed this process, transfecting individual plasmid DNAs with combinations of three or with all four constructs. Two days later, media were collected, cells were dissolved with detergent buffer, and any VLPs present in media were pelleted by ultracentrifugation. Finally, S, E, M, and N proteins in aliquots of cell lysates and VLPs were imaged by Western immunoblotting.

The results (Fig. 2) revealed several basic elements of this assembly system. First, the secretion of VLPs from 293T cells transfected with the S, E, M, and N cDNAs was prolific, with the majority of the soluble M protein assembly subunits being secreted (Fig. 2, lane 9). M proteins are the primary components of coronavirions, and their presence in medium is a key indicator of successful particle assembly and secretion. Second, secreted VLPs were prevalent with or without S proteins (Fig. 2, compare lanes 5 and 9). This second finding confirms previous results indicating that S is incorporated into virus particles when present, but is entirely dispensable for the assembly and secretion process (2, 51). Third, when synthesized alone, none of the virion proteins were identified in the VLP fraction (Fig. 2, lanes 1 to 4). This finding that E proteins in particular were not secreted suggested that the plasmid DNA-based assembly system is set apart from those in which E proteins are greatly overexpressed using replication-competent Sindbis virus vectors, where some of the overexpressed E proteins secreted into medium (33). Fourth, N proteins were required to accumulate secreted VLPs (Fig. 2, compare lanes 8 and 9). This is a significant result in light of earlier findings of nucleocapsid-independent MHV assembly (2, 51). These profound requirements for N proteins provide an additional distinction from those systems first used to establish components and parameters for coronavirus assembly, where membrane proteins were typically overexpressed using vaccinia virus vectors (51).

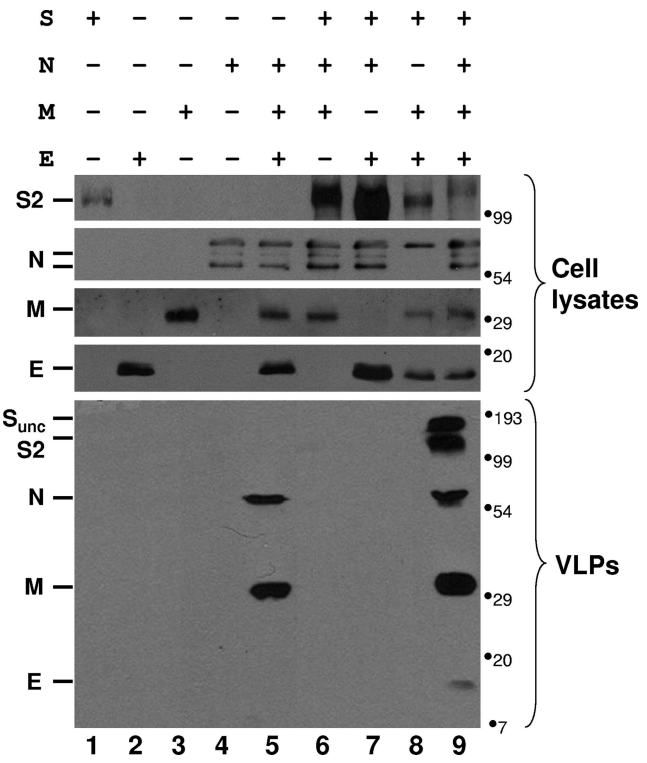

FIG. 2. Plasmid DNA-encoded VLP production. Parallel cultures of 10^6 293T cells were transfected with 1-μg amounts of pCAGGS plasmids encoding the indicated MHV (strain A59) proteins, as described in Materials and Methods. After 2 days, medium was collected and cells were dissolved in a lysis buffer containing NP-40 and deoxycholate, while VLPs in clarified medium was pelleted by ultracentrifugation. Viral proteins associated with the cell lysates, and VLPs were detected after their separation by SDS-PAGE and immunoblotting with antibodies specific for S, N, M, and E. S_{unc}, uncleaved ~180-kDa S protein precursor. S2, C-terminal S cleavage product. The positions of molecular mass markers are designated in kilodaltons at the right of each immunoblot panel.

Construction and evaluation of mutant E proteins. We focused on the E proteins because they have a central role in VLP and virion morphogenesis. Using site-specific mutagenesis and standard molecular biology techniques, we created two fundamental modifications to E genes. The first modifications involved epitope tagging. Given our limited supply of rabbit antibodies recognizing native E proteins, we chose to append coding sequences for HA epitopes at the 3′ open reading frame termini. Following transfections of 293T cells, untagged E and E_{HA} accumulated to similar levels, as estimated by Western immunoblotting (data not shown). In cotransfection with S, M, and N-encoding plasmids, E_{HA} fostered the secretion of VLPs (Fig. 3), indicating that this C-terminal epitope tag could be tolerated without destroying membrane morphogenetic functions.

The second modifications involved substituting cysteine residues in the cysteine-rich region to either alanines or glycines. We chose to replace cysteine with alanine or glycine instead of the more structurally analogous serine because these changes reflect the natural variation found among the coronavirus E proteins in this region (Fig. 1). Once constructed, the mutant E genes were evaluated for VLP morphogenetic capabilities by cotransfecting each into 293T cells along with S-, M-, and N-encoding plasmids. Immunoblot analyses of the virion proteins accumulated in 2 days revealed similar levels of S and N in cell lysates, with M proteins only faintly detected in all the transfectants except for those lacking E (Fig. 4, top panels, lanes 1 to 5). There were clearly variable levels of these same proteins in VLP preparations collected from medium (Fig. 4, bottom panel). Relative to native E proteins (Fig. 4, lane 2),

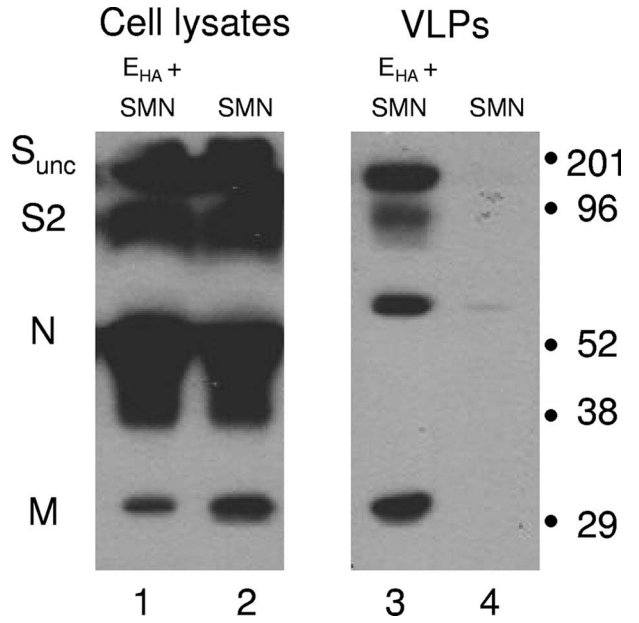

FIG. 3. Evaluation of HA-tagged E proteins in VLP assays. 293T cells were transfected with pCAGGS plasmids encoding the indicated proteins. E_{HA} encodes E with an appended C-terminal 9-amino-acid epitope. After 2 days, viral S, N, and M proteins were detected in cell lysate and VLP fractions as described in the legend for Fig. 2. The positions of molecular mass markers are designated in kilodaltons. S_{unc}, uncleaved ~180-kDa S protein precursor. S2, C-terminal S cleavage product.

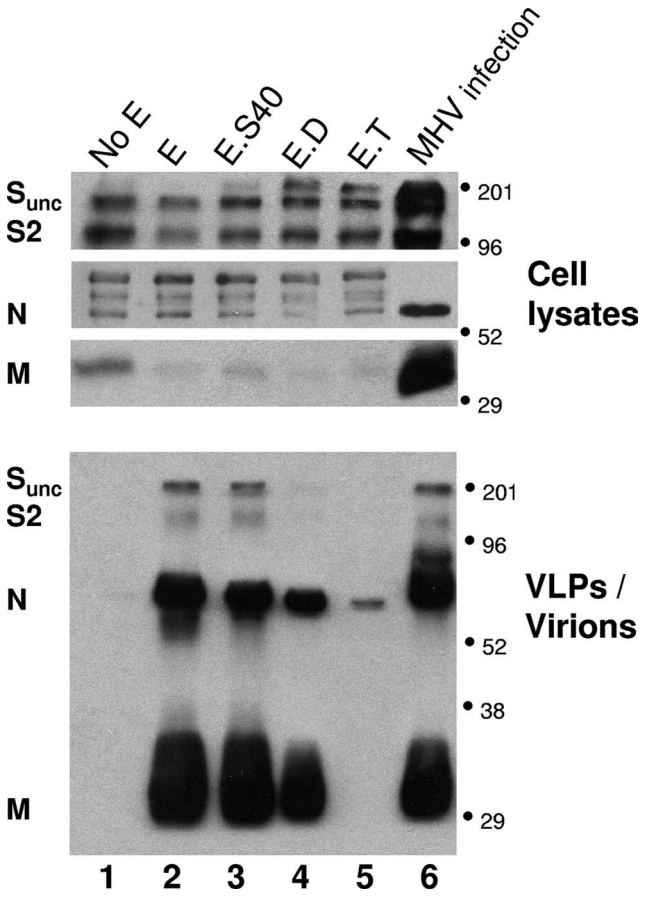

FIG. 4. Evaluation of mutant E proteins in VLP assays. 293T cells were transfected with pCAGGS plasmids encoding S, N, M, and the indicated E forms. E.S is E with the C40A substitution, E.D is E with the C40A/C44G substitution, and E.T is E with the C40A/C44G/C47G substitution. At 2 days posttransfection/infection, cells were dissolved and secreted VLPs or virions were pelleted by ultracentrifugation. S, N, and M proteins in cell lysates and secreted VLPs or virions were detected by Western immunoblotting to generate the bands in lanes 1 to 5. In parallel, a 293T cell culture identical to that described above was transfected with pcDNA3-CEACAM encoding the MHV receptor and infected 18 h later with authentic MHV strain A59 at a multiplicity of infection of 1. Proteins in cell lysates and secreted virions were then evaluated by Western immunoblotting to generate the bands in lane 6. In this assay, lysate-associated proteins were derived from 1/50 of each culture, whereas VLP and virion proteins were derived from 1/5 of each culture.

single-mutant E.S40 (C40A) proteins were similarly effective at creating VLPs (lane 3); in both cases, the abundance of secreted particles roughly equaled that obtained after natural MHV infection of mCEACAM-positive 293T cells (lane 6). The double-mutant E.D (C40A/C44G) proteins were clearly compromised (Fig. 4, lane 4), and triple-mutant E.T (C40A/C44G/C47G) (lane 5) proteins were entirely unable to act as VLP morphogens. The N protein band evident in the VLPs collected from cells with S, M, N, and E.T (Fig. 4, lane 5) was also observed when E was absent (lane 1) and is most likely derived from RNP complexes that copurified with VLPs after being liberated from a small proportion of dead cells. These findings indicated that more than one cysteine in this cysteine-rich region and, by inference, more than one palmitate adduct were necessary for the complete function of E proteins in VLP synthesis and/or secretion.

Comparing biochemical and cell biological properties of E_{HA} and $E.T_{HA}$. We focused on comparing functional E_{HA} with incompetent $E.T_{HA}$ by first assessing palmitoylation status. Established assays include metabolic labeling with ^{3}H palmitate and/or evaluation of electrophoretic mobility shifts following removal of thioester-linked palmitic acids (11). We selected the latter approach because the small E apoproteins would be approximately 8% larger with three covalently linked palmitates and, thus, likely resolve as distinct electrophoretic forms. Also, electrophoretic resolutions could provide estimates of the proportion of total E proteins that become post-translationally modified with palmitates. Thus, we exposed immunoprecipitated E proteins to hydroxylamine and assessed electrophoretic mobilities by Western immunoblotting. The results revealed roughly equal proportions of two distinct electrophoretic forms for the native E_{HA} proteins (Fig. 5, lane 1) but only the faster-migrating form for $E.T_{HA}$ (lane 2). After hydroxylamine exposures, only the faster-migrating forms were evident for both native E and E.T (Fig. 5, lanes 4 to 6). These results argue that only about one-half of the native E proteins received palmitate adducts, perhaps because plasmid DNAs express E so abundantly that they exceed cellular palmitoylation capacities. The results also support the important contention that E.T proteins exist only as nonpalmitoylated apoprotein forms.

Palmitoylation status can influence protein sorting within the cell (18, 29). Therefore, it was necessary to determine whether native E_{HA} and $E.T_{HA}$ occupied similar subcellular

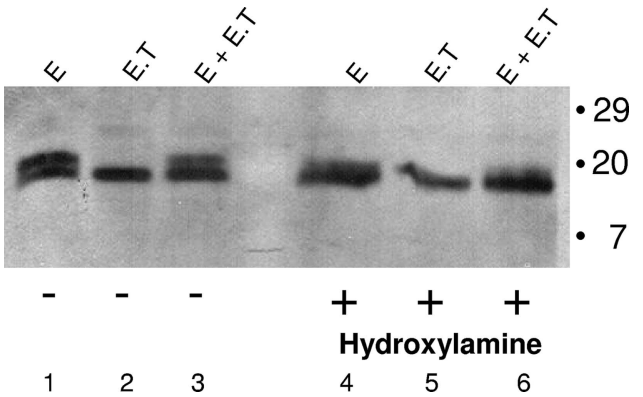

FIG. 5. Effect of hydroxylamine on E protein electrophoretic mobilities. 17Cl1 cells were lipofected with pCAGGS-E_{HA} or $E.T_{HA}$ and dissolved 24 h later in nonionic detergent-containing lysis buffer. E proteins in clarified cell lysates were then immunoprecipitated with anti-HA antibodies and dissolved in SDS solubilizer. Aliquots of the E_{HA}- and $E.T_{HA}$-containing samples were incubated either alone (−) or together (+) with 0.5 M hydroxylamine for 15 min, subjected to electrophoresis on 14% polyacrylamide gels, and then detected by immunoblotting using anti-HA antibodies.

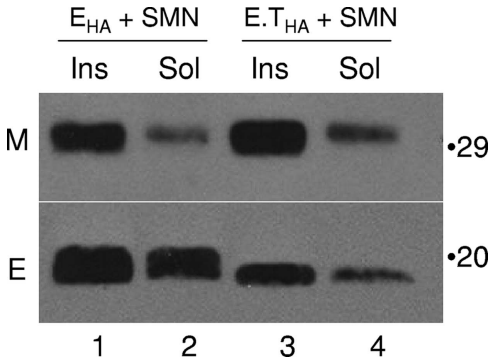

FIG. 7. Copurification of E and M proteins. 293T cells were transfected with plasmids encoding the indicated viral proteins. Two days later, cells were collected into lysis buffer and separated into insoluble (Ins) and soluble (Sol) fractions, as described in Materials and Methods. M and E proteins associated with the subcellular fractions were detected by immunoblotting with anti-M and anti-HA antibodies. Positions of the 29- and 20-kDa molecular mass markers are indicated at the right side of the immunoblot images.

locations. To this end, immunofluorescence assays were performed on E_{HA}-transfected and MHV-infected 17Cl1 cells. Using FITC-conjugated anti-HA antibodies, we observed striking perinuclear fluorescence signals in cells harboring E_{HA} or $E.T_{HA}$ (Fig. 6, left panels). Relative to the much wider distribution of N proteins, the immunofluorescence signals for E_{HA} and $E.T_{HA}$ appeared similarly localized. In a separate immunofluorescence assay, the subcellular distributions of Golgin-97 and E_{HA} were compared. Signals for Golgin-97, which mark Golgi vesicles, overlapped with both E_{HA} and $E.T_{HA}$ (Fig. 6, bracketed panels). In conjunction with the data for Fig. 5, these findings indicate that palmitate modifications are not the subcellular targeting agents on E proteins. Similar conclusions

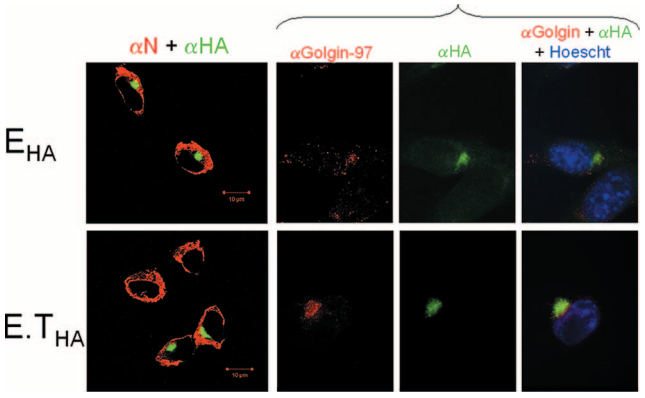

FIG. 6. Subcellular localization of E_{HA} and $E.T_{HA}$ proteins. 17Cl1 cells were lipofected with pCAGGS-E plasmids and subsequently infected with MHV A59. At 8 hpi, cells were fixed, permeabilized, and stained with FITC-conjugated anti-HA antibodies (green), with mouse anti-N antibodies, and with secondary Alexa 658 (red)-conjugated anti-mouse immunoglobulin antibodies. In a separate assay, E-transfected cells were stained with anti-HA (green) and anti-Golgin-97 and then with Alexa 658 (red)-conjugated antibodies. Images were captured by confocal microscopy.

were reached by Corse and Machamer in studies of IBV E proteins, in which they found E targeting to the Golgi complex independent of palmitoylation status (3).

A separate report by Corse and Machamer, demonstrating an association between IBV E and M (4), prompted us to consider whether the MHV E_{HA} and $E.T_{HA}$ proteins might be distinguished by their interactions with M. These putative associations were first evaluated by determining whether E and M proteins copurify in crude subcellular fractions of transfected 293T cells. Thus, cells expressing E and M proteins were disrupted with an NP-40 and deoxycholate (DOC)-containing buffer and the lysates were partitioned by centrifugation into detergent-insoluble and -soluble fractions. After adding SDS (which dissolved insoluble material) to these fractions, immunoblotting was used to identify E and M proteins. The majority of E and M proteins were in the NP-40-insoluble/DOC-insoluble fractions (Fig. 7), in accordance with the known detergent stability of multimeric M and S-M protein complexes (40, 53). It is important to note that these data do not reveal direct interactions between E and M proteins, but rather only that their copurification into detergent-insoluble pellets suggests similar biochemical properties for both palmitoylated and nonpalmitoylated E.

The E_{HA} proteins partitioned with M proteins in detergent-insoluble fractions, yet these protein combinations were also capable of secreting out of cells in VLPs. This capability was further documented with immunoblotting to estimate the proportion of M and E proteins in the insoluble and soluble cellular fractions relative to that found in secreted VLPs. In 293T cells at 2 days posttransfection, the vast majority of M proteins were within insoluble complexes when E was absent (Fig. 8, lanes 1 to 3) or when E.T was present (lanes 7 to 9), but in the presence of native E proteins, most M was mobilized into VLPs (lanes 4 to 6). The M proteins that secreted in VLPs contained an extremely small proportion of the slower-migrating, palmitoylated E, revealed only after chemiluminescence overexposure (Fig. 8, bottom panel, lane 6). These VLP-associated proteins were entirely detergent soluble (data not shown); this result was expected as it is well known that envel-

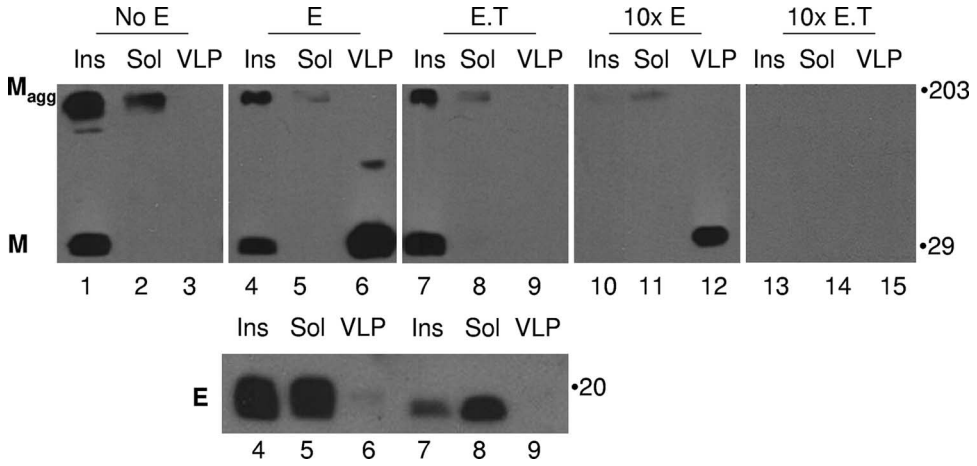

FIG. 8. Mobilization of M proteins from insoluble complexes by increasing E levels. 293T cells (10^6) were transfected with 1-μg amounts of pCAGGS plasmids encoding S, M, N, and either E or E.T. Where indicated, the input doses of E and E.T plasmids were increased 10-fold (10×), to 10 μg. After 2 days, cells were collected into lysis buffer and fractionated into insoluble (Ins) and soluble (Sol) material. VLPs were pelleted from medium by ultracentrifugation. Samples representing equivalent proportions of each culture were then subjected to immunoblotting to detect the M and E proteins. M_{agg}, SDS-insoluble M protein aggregates.

oped MHV particles are disrupted by low concentrations of nonionic detergent (48). Interestingly, when the proportion of E was increased by raising the pCAGGS-E input dose 10-fold, less M protein was recovered from cultures, but essentially all of it was associated with VLPs (Fig. 8, lanes 10 to 12). A corresponding 10-fold increase in E.T dose reduced M protein levels below detection limits and, notably, did not foster any M protein secretion (Fig. 8, lanes 13 to 15). Thus, the overexpression of E proteins reduces the accumulation of insoluble M protein aggregates and, notably, only the palmitoylated E proteins will mobilize M proteins out of cells and into detergent-soluble VLPs.

A straightforward complementation system. To evaluate the mutant E proteins in the context of a natural coronavirus infection, we employed complementation systems (5, 12, 42). To this end, we constructed an rA59 in which the initiation ATG codon for E was changed to TAG, knocking out E expression (rA59-Eko). To facilitate our complementation assays, the gene for FL was inserted between the E and M open reading frames, as was shown to us by de Haan et al. (8). This virus, rA59-Eko-FL-M, grew to titers ~1,000 times lower than those of the E-containing rA59-E-FL-M, in accordance with the known requirements for MHV E in assembly (26). The rAsq-E-FL-M was used in complementation tests, as schematically depicted in Fig. 9A. "Producer" 17Cl1 cells were lipofected with the various pCAGGS-E plasmids and infected 6 h later with rA59-Eko-FL-M. At 18 hpi, media were collected and used to inoculate fresh "target" 17c1l cells. Six hours later, FL accumulations were quantified in the target cells and the data were used to determine the extents of E protein complementation.

Our results (Fig. 9) revealed that native E increased producer cell output by a factor of ~1,000. E.S mutants with cysteine-to-alanine changes at position 40, 44, or 47 were all slightly reduced in complementation potential, arguing for the preservation of all these cysteines in MHV evolution. The E.D mutant was about 10-fold reduced, while the E.T mutant was entirely incapable of complementation. These impaired complementation capacities could not be explained by any failure to accumulate mutant E proteins in producer cells, as all E forms were similarly abundant, as estimated by immunoblot analyses (Fig. 9C). Thus, the abilities of E proteins to generate VLPs paralleled their capacities to complement rA59-Eko viruses.

Separate confirmation that E.T did not function in natural infection was achieved by constructing rA59-E.T-FL-M, which was indistinguishable from rA59-Eko-FL-M in all of our assays. The rA59-E.T-FL-M virus was similarly complemented by plasmid-derived E (Fig. 10). In turn, plasmid-derived E.T did not interfere with the output of the normal, E-encoding, rA59-E-FL-M (Fig. 10). Together, these results argue that E.T proteins neither support nor interfere with natural MHV infections.

The discovery that increased E gene doses assisted M protein mobilization out of insoluble intracellular aggregates (Fig. 8) prompted us to consider whether preexisting E proteins in 17Cl1 producer cells would increase output of MHV. Thus, we extended complementation tests to include infection by rA59-E-FL-M. Here we found that preexisting E proteins did not have any influence on the replication of the rA59-E-FL-M, as measured by FL accumulations in producer cells (Fig. 11A). This result accorded with the fact that E has no role in the viral replication process (26). But preexisting E did increase virus output about 10-fold, as revealed by FL accumulations in secondarily infected targets (Fig. 11B). These findings demonstrate that E proteins can prime cells for more rapid assembly and/or secretion of progeny virus particles.

DISCUSSION

The essential findings in this report indicate that E proteins must be palmitoylated posttranslationally to function in virion assembly. Palmitoylations are therefore required on both E proteins and S proteins (50) to achieve efficient virus assembly. These findings attest to the role of cellular palmitoyl acyltransferases as cofactors in productive coronavirus infection. These

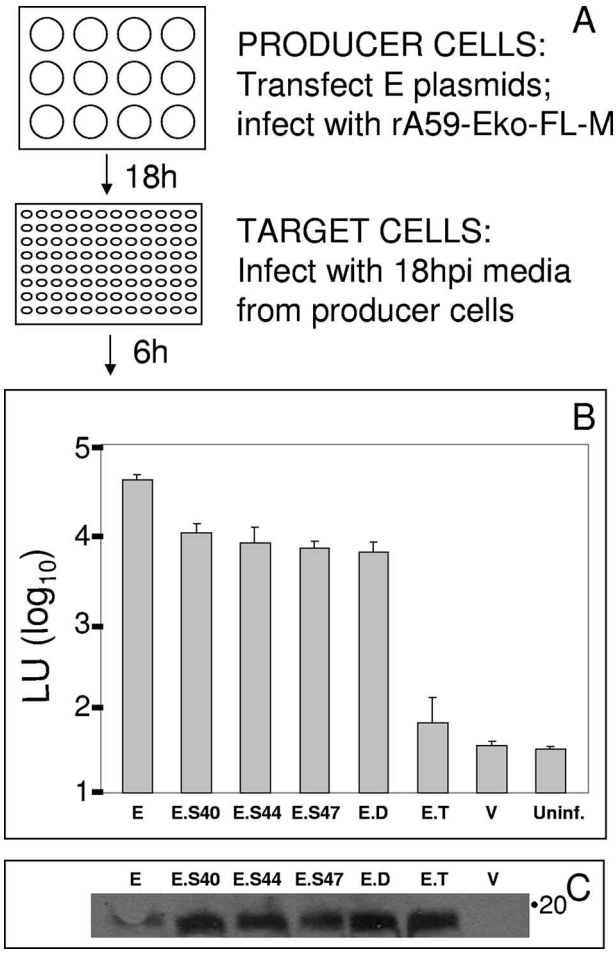

FIG. 9. Complementation of rA59-Eko-FL-M by plasmid-encoded E proteins. As schematically depicted in panel A, 17Cl1 cells were lipofected with the indicated pCAGGS-E constructs and infected 6 h later with rA59-Eko-FL-M (0.004 PFU/cell). After 18 h, medium was collected from producer cells, clarified, and used to inoculate 17Cl1 target cells. At 6 hpi, target cells were lysed. Luciferase light units (LU) in target cell lysates are plotted in panel B. Each data point represents the average luciferase levels from three parallel lipofection infection assays. V, data obtained from empty pCAGGS vector-transfected cultures. Uninf, data obtained from uninfected control cultures. Panel C depicts E protein-specific signals obtained after Western immunoblot analysis of the indicated producer cell lysates that were collected at 18 hpi. Error bars indicate standard deviations.

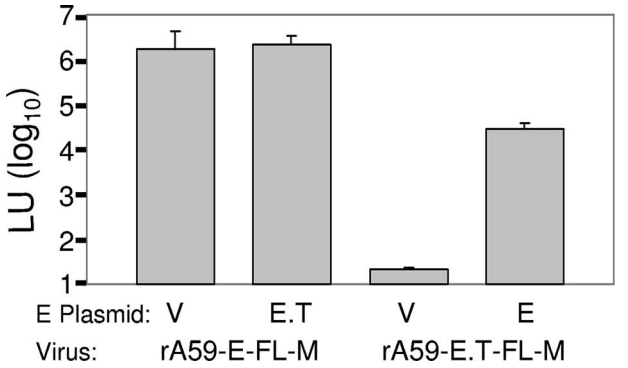

FIG. 10. Complementation of rA59-E- and E.T-FL-M by plasmid-encoded E proteins. Complementation assays were performed as described in the legend for Fig. 9, with rA59-Eko replaced by the indicated recombinant viruses. Luciferase (LU) data points represent the average of the values obtained from three parallel complementation assays. V, data obtained from empty pCAGGS vector-transfected cultures.

findings also suggest that virion proteins arrange on membranes in relation to their palmitoylation status (Fig. 1) and, in doing so, become functional assembly components.

Approaches to evaluate virus assembly. The approaches we used to evaluate MHV assembly were particularly facile in revealing E functions. The plasmid DNA-based approach to manufacturing VLPs was robust and reflective of the natural MHV virion assembly process (Fig. 2 and 4). Notably, this VLP assembly process was profoundly dependent on E, M, and N proteins, with the requirements for N being similar to the SARS coronavirus assembly system described previously by Huang et al. (21) but different from findings obtained by Vennema et al. (51). With respect to this N dependence, our view is that N proteins, or helical N-to-RNA RNP complexes, provide templates for condensing membrane proteins S, E, and M. N-M and M-S interactions are well documented (35), making the repeating N subunits on RNPs attractive candidates to arrange membrane proteins at virion budding sites. Accordingly, the VLP assembly system could become less dependent on N proteins as S, E, and M protein levels increase. Thus, we suggest that our findings are in concert with the seminal discoveries of Vennema et al. (51), who originally found that N proteins were not required for MHV VLP assembly when vaccinia virus vectors expressed the MHV genes. Vaccinia virus-mediated overexpression may lead to accumulations high enough for S, M, and E proteins to meet up within intracellular membranes without a unifying cytoplasmic scaffold of N proteins or RNPs. Overexpression, however, may create certain biologically irrelevant features, inasmuch as assembly without RNPs would secrete "empty" noninfectious particles. In a natural infection, there may be no time at which the membrane proteins S, E, and M accumulate in stoichiometric excess over that of the N proteins. This likelihood, in conjunction with the understanding that N proteins catalyze assembly, reduces the plausibility of empty particle formation during natural infections.

The plasmid DNA-based VLP assembly system has obvious utility in revealing the morphogenetic capabilities of E proteins. We observed stepwise declines in morphogenetic capacity with increasing cysteine substitutions (Fig. 4 and 9), pointing to palmitoylation-dependent assembly and also providing an explanation for more than one cysteine in this region of the coronavirus E proteins (Fig. 1 shows amino acid sequences). The VLP production patterns also correlated with authentic virus production patterns in E complementation assays (Fig. 9), making it clear that the VLP approach to evaluating assembly faithfully mimics the natural process taking place in MHV-infected cells.

Current views of E protein function. The coronavirus E protein can be confidently designated as a virion morphogenetic factor (7, 35); however, there can be two distinct viewpoints regarding the specific functions of the E protein during the assembly process. One position is that the E protein is a

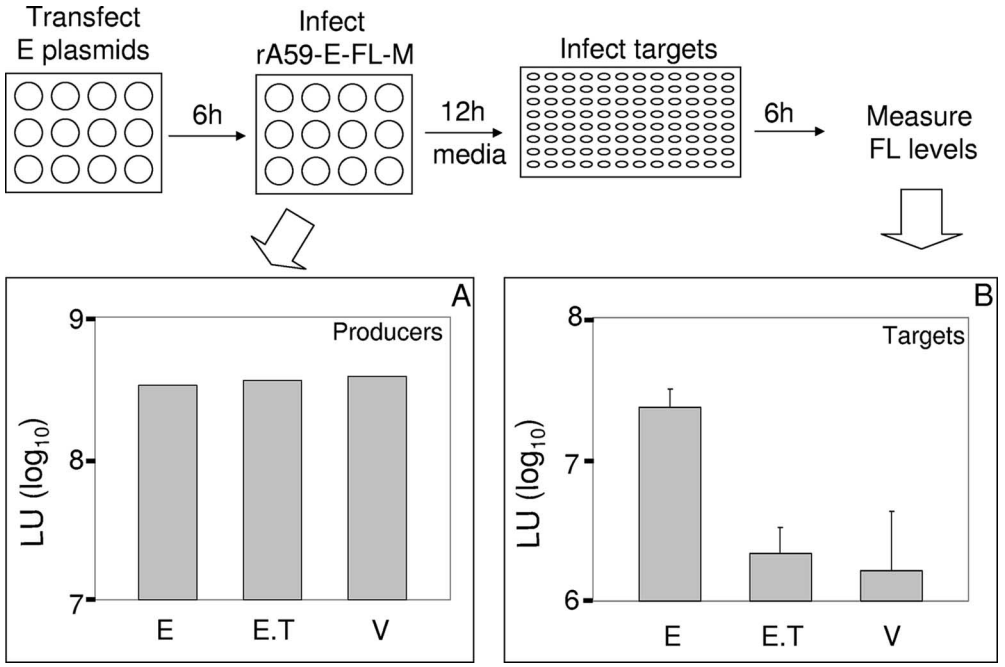

FIG. 11. Augmentation of rA59-E-FL-M assembly/secretion by plasmid-encoded E proteins. 17Cl1 producer cells were transfected with pCAGGS-E plasmids as indicated. Six hours later, the cells were infected with rA59-E-FL-M virus and, at 12 hpi, media were collected and producer cells were lysed for determination of luciferase accumulations. The medium was then clarified and used to infect 17Cl1 target cells, which were lysed at 6 hpi and evaluated for luciferase accumulations using a plate-reading luminometer. Error bars indicate standard deviations. V, data obtained from empty pCAGGS vector-transfected cultures.

fundamental, essential structural component of the coronavirus particle. This outlook is supported by the facts that E is indeed present in progeny virus particles (58), that E proteins can be cross-linked to the M proteins that comprise the primary subunits of coronavirions (4), and that E mutations significantly influence the morphologies of secreted virus particles (14). A second, contrasting viewpoint is that E proteins are not true "structural" components, that rather, they are only incidentally incorporated into progeny virions because their accumulation on intracellular membranes happens to overlap with sites of virion budding. This second view is modestly supported by the fact that E proteins accumulate to copious levels within infected cells, yet only an extremely small fraction secrete with virions (Fig. 2 and 8). Another attraction to this second viewpoint derives from the absence of any obvious role for E proteins in the context of secreted virions. Virions entirely devoid of E proteins can be constructed (6, 26), and while these delta E particles are not abundantly made, they are infectious as measured by conventional plaque assays, leading one to suspect that there is no special role for E proteins in virions or during the virus entry process. One can be further influenced by another elegant study from the Masters laboratory (24) in which divergent E proteins from various coronaviruses were each found to function in complementing MHVs lacking their endogenous E. This result clearly argues against E proteins evolving in concert with M and S proteins, that is, against virus-strain-specific E-M structural units in the assembled virion.

In this second perspective, the E proteins might be viewed as agents that generally reshape intracellular membranous organelles, in doing so, somehow accommodating facile budding and the secretion of coronavirus particles. Indeed there is evidence that E proteins remodel intracellular membranes, their synthesis correlating with novel elongated and distended vesicles (44) and with fragmented Golgi membranes (41). Precisely how the E proteins achieve this remodeling, and whether host factors are recruited in the process, is not yet known. It is known that the E proteins of both MHV and SARS coronaviruses exhibit in vitro ion channel activities (32, 54, 55), and therefore, it is conceivable that oligomeric E protein pores might alter the tonicities within organelle lumens and thus inflate vesicles enough to accommodate budding and exocytosis of coronavirions. There is abundant literature addressing the hypothesis that virus-encoded ion channels, i.e., "viroporins," are somehow involved in mediating virus assembly and release from cells (17, 31).

New insights on E protein function. Our results can be succinctly summarized as follows. E proteins with three cysteine substitutions, designated E.T, were unchanged in electrophoretic mobility by hydroxylamine treatments (Fig. 5) and thus were likely devoid of palmitate adducts. This absence of palmitoylation did not change E subcellular localization (Fig. 6) or copurification with M in detergent-insoluble protein complexes (Fig. 7) but did eliminate E competence in VLP and authentic virus assembly (Fig. 4 and 9). Increased levels of the native, palmitoylated E proteins reduced the proportion of M proteins in detergent-insoluble complexes (Fig. 8) and also primed cells for robust virus secretion (Fig. 11). These findings bring new insights into the operating mechanisms of E proteins.

The first insight bears on the hypothesis that E proteins function as ion channels to promote coronavirus assembly. It is important to remember that evidence for ion channels was obtained by intercalating nonpalmitoylated E peptides into model membrane bilayers and subsequently measuring peptide-induced conductances. Cation-specific channel activities were observed, and in the case of the MHV E-induced pores, conductances were diminished by hexamethylene amiloride, a well-known inhibitor of Na^+/K^+ antiporters. The findings in our report cast no doubt on these electrophysiological studies documenting E protein ion channels. However, in our view, there are at least two reasons to question whether E proteins must be ion channels to foster virus assembly. First, nonpalmitoylated E proteins were the forms that generated in vitro ion channel activities, but these forms cannot function in the context of a natural infection, making it clear that if channels do arise in infected cells, some additional function dependent on palmitoylation must also be present to foster virus assembly. Second, in extending the findings of Wilson et al. (54), we applied hexamethylene amiloride during MHV infections, but we found that this drug suppressed E-containing rA59-E-FL-M and rA59-Eko-FL-M equally (data not shown), making us conclude that hexamethylene amiloride has confounding targets in addition to E. For these reasons, we are skeptical of the hypothesis that the E ion channel activities are central to their virion morphogenetic activity.

The second insight relates to the way in which E proteins mobilized M proteins out of detergent-insoluble complexes. These findings lead us to suggest that E proteins act as emulsifying agents, preventing M proteins from connecting together into denatured aggregates. It is conceivable that E proteins intersperse between M proteins to interrupt an otherwise hyperstable M protein lattice-like network, thereby permitting enough flexibility for virus budding. A reasonable view is that E palmitoylation is required for this emulsifying property because the lipid adducts force a more oblique arrangement relative to membranes, as is suggested in Fig. 1. Perhaps these E arrangements cause membrane curvature or dictate the spacing of M proteins. It remains to be determined whether those coronavirus assembly reactions that are profoundly E dependent, e.g., TGEV (5, 42), involve M proteins with the greatest tendencies for unproductive aggregation. Clearly there is more to learn through further comparison of different coronavirus assembly processes and through high-resolution imaging of coronavirus membrane protein organizations (37).

In analogy to MHV E, there are several cellular palmitoylated proteins participating in membrane reshaping (1); among these are caveolae-associated caveolins and endoplasmic-reticulum-associated reticulons. These small cellular proteins insert hydrophobic hairpin-like sequences and nearby palmitates into cytoplasmically facing membrane leaflets, which likely induces "positive" membrane curvatures, forming caveolae and endoplasmic reticulum tubules. Coronavirus E proteins have no primary sequence homologies to caveolae or reticulons, but their obvious similarities in hydrophobic stretches, lipid adducts, and membrane insertions suggest that these cellular motifs are captured by viruses to create the opposite "negative" membrane curvatures necessary to form extracellular virion vesicles. That viruses may utilize these motifs for membrane-reshaping "negative" membrane curvatures is supported by the palmitoylated R peptides of certain retroviruses that are proposed to induce budding (39). Additional noteworthy examples include the reovirus fusion-associated small transmembrane peptides. Palmitoylated cysteines juxtaposed near the transmembrane spans of these ~100-residue, fusion-associated small transmembrane peptides are required to induce negative curvatures at plasma membranes and resulting cell-cell fusions (46). There are also a plethora of much larger viral membrane proteins participating in virus entry as mediators of virus-cell and cell-cell membrane fusions. These include coronavirus S, myxovirus hemagglutinin, and retrovirus envelope proteins. Although there are notable exceptions, the membrane fusion activities of these proteins are generally augmented by palmitate modifications at cysteines near the boundary between hydrophobic membrane-intercalating and cytoplasmic residues (13, 43, 56). Such arrangements of lipophilic peptide and nearby attached lipid(s) may comprise part of a useful membrane-bending motif. Additional discoveries that these sorts of structures are indeed general membrane-bending elements would offer a satisfying explanation for their presence in many of the remodeling events that are fundamental to enveloped virus assembly and entry.

ACKNOWLEDGMENTS

We thank Shinji Makino (University of Texas-Galveston), Fumihiro Taguchi (National Institute of Infectious Diseases, Tokyo, Japan), and John Fleming (University of Wisconsin—Madison) for antiviral antibodies. We also thank Paul Masters (Wadsworth Center, New York State Department of Health) for pMH54 DNA and FCWF cells.

REFERENCES

1. **Bauer, M., and L. Pelkmans.** 2006. A new paradigm for membrane-organizing and -shaping scaffolds. FEBS Lett. **580:**5559–5564.
2. **Bos, E. C., W. Luytjes, H. V. van der Meulen, H. K. Koerten, and W. J. Spaan.** 1996. The production of recombinant infectious DI-particles of a murine coronavirus in the absence of helper virus. Virology **218:**52–60.
3. **Corse, E., and C. E. Machamer.** 2002. The cytoplasmic tail of infectious bronchitis virus E protein directs Golgi targeting. J. Virol. **76:**1273–1284.
4. **Corse, E., and C. E. Machamer.** 2003. The cytoplasmic tails of infectious bronchitis virus E and M proteins mediate their interaction. Virology **312:**25–34.
5. **Curtis, K. M., B. Yount, and R. S. Baric.** 2002. Heterologous gene expression from transmissible gastroenteritis virus replicon particles. J. Virol. **76:**1422–1434.
6. **DeDiego, M. L., E. Alvarez, F. Almazan, M. T. Rejas, E. Lamirande, A. Roberts, W. J. Shieh, S. R. Zaki, K. Subbarao, and L. Enjuanes.** 2007. A severe acute respiratory syndrome coronavirus that lacks the E gene is attenuated in vitro and in vivo. J. Virol. **81:**1701–1713.
7. **de Haan, C. A., and P. J. Rottier.** 2005. Molecular interactions in the assembly of coronaviruses. Adv. Virus Res. **64:**165–230.
8. **de Haan, C. A., L. van Genne, J. N. Stoop, H. Volders, and P. J. Rottier.** 2003. Coronaviruses as vectors: position dependence of foreign gene expression. J. Virol. **77:**11312–11323.
9. **de Haan, C. A., H. Vennema, and P. J. Rottier.** 2000. Assembly of the coronavirus envelope: homotypic interactions between the M proteins. J. Virol. **74:**4967–4978.
10. **de Haan, C. A. M., M. Smeets, F. Vernooij, H. Vennema, and P. J. M. Rottier.** 1999. Mapping of the coronavirus membrane protein domains involved in interaction with the spike protein. J. Virol. **73:**7441–7452.
11. **Drisdel, R. C., J. K. Alexander, A. Sayeed, and W. N. Green.** 2006. Assays of protein palmitoylation. Methods **40:**127–134.
12. **Eriksson, K. K., D. Makia, R. Maier, L. Cervantes, B. Ludewig, and V. Thiel.** 2006. Efficient transduction of dendritic cells using coronavirus-based vectors. Adv. Exp. Med. Biol. **581:**203–206.
13. **Fischer, C., B. Schroth-Diez, A. Herrmann, W. Garten, and H. D. Klenk.** 1998. Acylation of the influenza hemagglutinin modulates fusion activity. Virology **248:**284–294.
14. **Fischer, F., C. F. Stegen, P. S. Masters, and W. A. Samsonoff.** 1998. Analysis of constructed E gene mutants of mouse hepatitis virus confirms a pivotal role for E protein in coronavirus assembly. J. Virol. **72:**7885–7894.
15. **Fleming, J. O., S. A. Stohlman, R. C. Harmon, M. M. C. Lai, J. A. Frelinger,**

and L. P. Weiner. 1983. Antigenic relationships of murine coronaviruses: analysis using monoclonal antibodies to JHM (MHV-4) virus. Virology **131:** 296–307.
16. **Godeke, G. J., C. A. de Haan, J. W. Rossen, H. Vennema, and P. J. Rottier.** 2000. Assembly of spikes into coronavirus particles is mediated by the carboxy-terminal domain of the spike protein. J. Virol. **74:**1566–1571.
17. **Gonzalez, M. E., and L. Carrasco.** 2003. Viroporins. FEBS Lett. **552:**28–34.
18. **Greaves, J., and L. H. Chamberlain.** 2007. Palmitoylation-dependent protein sorting. J. Cell Biol. **176:**249–254.
19. **Grosse, B., and S. G. Siddell.** 1994. Single amino acid changes in the S2 subunit of the MHV surface glycoprotein confer resistance to neutralization by S1 subunit-specific monoclonal antibody. Virology **202:**814–824.
20. **Hofmann, H., K. Hattermann, A. Marzi, T. Gramberg, M. Geier, M. Krumbiegel, S. Kuate, K. Uberla, M. Niedrig, and S. Pohlmann.** 2004. S protein of severe acute respiratory syndrome-associated coronavirus mediates entry into hepatoma cell lines and is targeted by neutralizing antibodies in infected patients. J. Virol. **78:**6134–6142.
21. **Huang, Y., Z. Y. Yang, W. P. Kong, and G. J. Nabel.** 2004. Generation of synthetic severe acute respiratory syndrome coronavirus pseudoparticles: implications for assembly and vaccine production. J. Virol. **78:**12557–12565.
22. **Kida, Y., F. Morimoto, K. Mihara, and M. Sakaguchi.** 2006. Function of positive charges following signal-anchor sequences during translocation of the N-terminal domain. J. Biol. Chem. **281:**1152–1158.
23. **Kuo, L., G. J. Godeke, M. J. Raamsman, P. S. Masters, and P. J. Rottier.** 2000. Retargeting of coronavirus by substitution of the spike glycoprotein ectodomain: crossing the host cell species barrier. J. Virol. **74:**1396–1406.
24. **Kuo, L., K. R. Hurst, and P. S. Masters.** 2007. Exceptional flexibility in the sequence requirements for coronavirus small envelope protein function. J. Virol. **81:**2249–2262.
25. **Kuo, L., and P. S. Masters.** 2002. Genetic evidence for a structural interaction between the carboxy termini of the membrane and nucleocapsid proteins of mouse hepatitis virus. J. Virol. **76:**4987–4999.
26. **Kuo, L., and P. S. Masters.** 2003. The small envelope protein E is not essential for murine coronavirus replication. J. Virol. **77:**4597–4608.
27. **Laude, H., and P. S. Masters.** 1995. The coronavirus nucleocapsid protein, p. 141–163. *In* S. G. Siddell (ed.), The Coronaviridae. Plenum Press, New York, NY.
28. **Lim, K. P., and D. X. Liu.** 2001. The missing link in coronavirus assembly. Retention of the avian coronavirus infectious bronchitis virus envelope protein in the pre-Golgi compartments and physical interaction between the envelope and membrane proteins. J. Biol. Chem. **276:**17515–17523.
29. **Linder, M. E., and R. J. Deschenes.** 2007. Palmitoylation: policing protein stability and traffic. Nat. Rev. Mol. Cell Biol. **8:**74–84.
30. **Lontok, E., E. Corse, and C. E. Machamer.** 2004. Intracellular targeting signals contribute to localization of coronavirus spike proteins near the virus assembly site. J. Virol. **78:**5913–5922.
31. **Lu, W., B. J. Zheng, K. Xu, W. Schwarz, L. Du, C. K. Wong, J. Chen, S. Duan, V. Deubel, and B. Sun.** 2006. Severe acute respiratory syndrome-associated coronavirus 3a protein forms an ion channel and modulates virus release. Proc. Natl. Acad. Sci. USA **103:**12540–12545.
32. **Madan, V., J. Garcia Mde, M. A. Sanz, and L. Carrasco.** 2005. Viroporin activity of murine hepatitis virus E protein. FEBS Lett. **579:**3607–3612.
33. **Maeda, J., A. Maeda, and S. Makino.** 1999. Release of coronavirus E protein in membrane vesicles from virus-infected cells and E protein-expressing cells. Virology **263:**265–272.
34. **Maeda, J., J. F. Repass, A. Maeda, and S. Makino.** 2001. Membrane topology of coronavirus E protein. Virology **281:**163–169.
35. **Masters, P. S.** 2006. The molecular biology of coronaviruses. Adv. Virus Res. **66:**193–292.
36. **Masters, P. S., and P. J. Rottier.** 2005. Coronavirus reverse genetics by targeted RNA recombination. Curr. Top. Microbiol. Immunol. **287:**133–159.
37. **Neuman, B. W., B. D. Adair, C. Yoshioka, J. D. Quispe, G. Orca, P. Kuhn, R. A. Milligan, M. Yeager, and M. J. Buchmeier.** 2006. Supramolecular architecture of severe acute respiratory syndrome coronavirus revealed by electron cryomicroscopy. J. Virol. **80:**7918–7928.
38. **Niwa, H., K. Yamamura, and J. Miyazaki.** 1991. Efficient selection for high-expression transfectants with a novel eukaryotic vector. Gene **108:**193–199.
39. **Olsen, K. E., and K. B. Andersen.** 1999. Palmitoylation of the intracytoplasmic R peptide of the transmembrane envelope protein in Moloney murine leukemia virus. J. Virol. **73:**8975–8981.
40. **Opstelten, D.-J. E., M. J. B. Raamsman, K. Wolfs, M. C. Horzinek, and P. J. M. Rottier.** 1995. Envelope glycoprotein interactions in coronavirus assembly. J. Cell Biol. **131:**339–349.
41. **Ortego, J., J. E. Ceriani, C. Patino, J. Plana, and L. Enjuanes.** 2007. Absence of E protein arrests transmissible gastroenteritis coronavirus maturation in the secretory pathway. Virology **368:**296–308.
42. **Ortego, J., D. Escors, H. Laude, and L. Enjuanes.** 2002. Generation of a replication-competent, propagation-deficient virus vector based on the transmissible gastroenteritis coronavirus genome. J. Virol. **76:**11518–11529.
43. **Petit, C. M., V. N. Chouljenko, A. Iyer, R. Colgrove, M. Farzan, D. M. Knipe, and K. G. Kousoulas.** 2007. Palmitoylation of the cysteine-rich endodomain of the SARS-coronavirus spike glycoprotein is important for spike-mediated cell fusion. Virology **360:**264–274.
44. **Raamsman, M. J., J. K. Locker, A. de Hooge, A. A. de Vries, G. Griffiths, H. Vennema, and P. J. Rottier.** 2000. Characterization of the coronavirus mouse hepatitis virus strain A59 small membrane protein E. J. Virol. **74:**2333–2342.
45. **Risco, C., I. M. Anton, L. Enjuanes, and J. L. Carrascosa.** 1996. The transmissible gastroenteritis coronavirus contains a spherical core shell consisting of M and N proteins. J. Virol. **70:**4773–4777.
46. **Shmulevitz, M., J. Salsman, and R. Duncan.** 2003. Palmitoylation, membrane-proximal basic residues, and transmembrane glycine residues in the reovirus p10 protein are essential for syncytium formation. J. Virol. **77:**9769–9779.
47. **Siddell, S. G. (ed.)** 1995. The Coronaviridae, p. 1–10. Plenum Press, New York, NY.
48. **Sturman, L. S., K. V. Holmes, and J. Behnke.** 1980. Isolation of coronavirus envelope glycoproteins and interaction with the viral nucleocapsid. J. Virol. **33:**449–462.
49. **Swift, A. M., and C. E. Machamer.** 1991. A Golgi retention signal in a membrane-spanning domain of coronavirus E1 protein. J. Cell Biol. **115:** 19–30.
50. **Thorp, E. B., J. A. Boscarino, H. L. Logan, J. T. Goletz, and T. M. Gallagher.** 2006. Palmitoylations on murine coronavirus spike proteins are essential for virion assembly and infectivity. J. Virol. **80:**1280–1289.
51. **Vennema, H., G. J. Godeke, J. W. Rossen, W. F. Voorhout, M. C. Horzinek, D. J. Opstelten, and P. J. Rottier.** 1996. Nucleocapsid-independent assembly of coronavirus-like particles by co-expression of viral envelope protein genes. EMBO J. **15:**2020–2028.
52. **Wahlberg, J. M., and M. Spiess.** 1997. Multiple determinants direct the orientation of signal-anchor proteins: the topogenic role of the hydrophobic signal domain. J. Cell Biol. **137:**555–562.
53. **Weisz, O. A., A. M. Swift, and C. E. Machamer.** 1993. Oligomerization of a membrane protein correlates with its retention in the Golgi complex. J. Cell Biol. **122:**1185–1196.
54. **Wilson, L., P. Gage, and G. Ewart.** 2006. Hexamethylene amiloride blocks E protein ion channels and inhibits coronavirus replication. Virology **353:**294–306.
55. **Wilson, L., C. McKinlay, P. Gage, and G. Ewart.** 2004. SARS coronavirus E protein forms cation-selective ion channels. Virology **330:**322–331.
56. **Yang, C., C. P. Spies, and R. W. Compans.** 1995. The human and simian immunodeficiency virus envelope glycoprotein transmembrane subunits are palmitoylated. Proc. Natl. Acad. Sci. USA **92:**9871–9875.
57. **Ye, R., C. Montalto-Morrison, and P. S. Masters.** 2004. Genetic analysis of determinants for spike glycoprotein assembly into murine coronavirus virions: distinct roles for charge-rich and cysteine-rich regions of the endodomain. J. Virol. **78:**9904–9917.
58. **Yu, X., W. Bi, S. R. Weiss, and J. L. Leibowitz.** 1994. Mouse hepatitis virus gene 5b protein is a new virion envelope protein. Virology **202:**1018–1023.